Thin Solid Films 519 (2011) 6126–6129

Contents lists available at ScienceDirect

Thin Solid Films

journal homepage: www.elsevier.com/locate/tsf

Carbon nanotube forest growth on NiTi shape memory alloy thin films for thermal actuation

B.C. Bayer [a,*], S. Sanjabi [b], C. Baehtz [c], C.T. Wirth [a], S. Esconjauregui [a], R.S. Weatherup [a], Z.H. Barber [b], S. Hofmann [a], J. Robertson [a]

[a] Department of Engineering, University of Cambridge, Cambridge, CB3 0FA, UK
[b] Department of Materials Science and Metallurgy, University of Cambridge, Cambridge, CB2 3QZ, UK
[c] Institute of Ion Beam Physics and Materials Research, Helmholtz-Zentrum Dresden Rossendorf, Dresden, D-01314, Germany

ARTICLE INFO

Article history:
Received 26 August 2010
Received in revised form 11 March 2011
Accepted 16 March 2011
Available online 31 March 2011

Keywords:
Carbon nanotubes
Shape memory alloys
Chemical vapour deposition
NiTi
Thermal management

ABSTRACT

Actuation frequencies in thermally triggered Shape Memory Alloy (SMA) thin films are limited by the slow heat transport into/out of the films. Carbon Nanotubes (CNTs) are known to exhibit an exceptionally high thermal conductivity. Thus, we propose to thermally contact SMA films with CNTs to increase SMA actuation frequencies by enhanced heat transport through the CNTs. The basic requirement for this envisaged nanotube application is to obtain CNT forest growth on a SMA material while retaining a reversible martensitic transformation, as required for Shape Memory Effect exploitation. We show how such growth can be achieved on thin films of the SMA material NiTi. Future work is needed to measure thermal properties and obtainable cycling frequencies of CNT-SMA structures.

1. Introduction

Shape memory alloy (SMA) thin films are used for actuation in micro-electro-mechanical systems (MEMS) as they exhibit a temperature change triggered, reversible shape transformation with large strain (shape memory effect, SME) [1]. The occurrence of a higher symmetry, high temperature phase (austenite) and a lower symmetry, low temperature phase (martensite), allows that, after cooling from austenite to martensite, mechanical deformations in the martensite are reversible simply by heating back into the austenite regime. This leads to a one-way SME, where the shape of the austenite is "memorised". By appropriate "training" a two-way SME allows cycling between two shapes by temperature changes [1] and hence repeatable actuation, where SMAs possess orders of magnitude higher obtainable strains and associated forces compared to e.g. piezoelectrics [2]. However the possible cycling frequencies are limited by the slow heat transport into/out of the SMA to heat above/cool below the austenitic/martensitic transformation temperatures [1]. Thus, the use of high thermal conductivity materials as heat transport paths into/out of the SMA was suggested to allow higher cycling frequencies [3], however actual choice of such materials remains unclear.

Carbon nanotubes (CNTs) have been reported to have exceptionally high thermal conductivities of ~3000–6000 W/Km. [4,5] and are therefore promising as an efficient heat transport material. Thus, we now propose to combine SMAs and CNTs to increase cycling frequencies of SMA films by the enhanced heat transport through CNTs. While graphitic structures were recently identified to improve thermal transport in the field of polymer-based shape memory composites [6,7] and CNTs have been studied as thermal management materials in miroelectronics [8–17], our proposed approach of growth of CNTs by Chemical Vapour Deposition (CVD) directly onto metal-alloy SMA films for improved thermal actuation has not been considered so far.

Fig. 1 schematically shows our proposed layer structure, where CNTs enhance heat conduction from the SMA to a heat sink/source compared to other filler materials. As CNTs have anisotropic thermal conduction with the exceptional values only along the tube axis, CNTs in our scheme need to be of vertically aligned ("forest") form. This translates to a sufficiently high density of CNTs for self-organization through Van-der-Waals interactions [18], with the forest height comparable to the μm-scale architecture of MEMS. Additionally the CNT CVD must not impede the SMA films' desired SME properties which, in a first approximation, are characterised by the possibility of obtaining a reversible martensitic transformation. Hence, the CVD process should either leave the crystallographic structure of the SMA unaffected or even improve it towards obtaining a SME.

It has however proven difficult to retain a functional support material's functionality at the high temperatures and in the reactive gases during CNT growth. Various material interactions such as undesirable alloying, oxidation or carbide formation, all of which are

* Corresponding author.
E-mail address: bcb25@cam.ac.uk (B.C. Bayer).

0040-6090/$ – see front matter © 2011 Elsevier B.V. All rights reserved.
doi:10.1016/j.tsf.2011.03.044

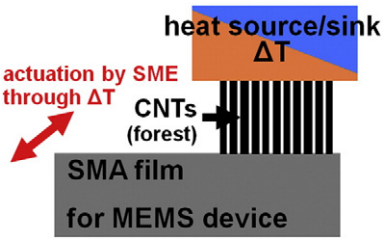

Fig. 1. Schematic of CNT forests as a high thermal conduction path material for thermally contacting SMA thin films to heat sources/sinks.

detrimental to functionality, have been found with metallic support films [19]. Hence the first necessary step for realisation of our proposed concept is to grow CNTs in forest form on a SMA material without losing the SME capability. Using the most extensively studied SMA, NiTi, we show that such growth can be achieved. Future work will need to deal with measurement of thermal properties and cycling frequencies of the CNT-SMA structures.

2. Experimental details

We first room temperature sputter deposit Ni-rich ($Ni_{\sim 51\ at.\%}Ti_{\sim 49\ at.\%}$) and Ti-rich ($Ni_{\sim 49\ at.\%}Ti_{\sim 51\ at.\%}$) NiTi thin films (~2 μm) onto r-plane sapphire substrates with a multi-gun sputter deposition system [20–22]. Note that martensitic transition temperatures in NiTi vary by tens of °C with just minor changes in atomic composition [2], allowing us to probe below and above room temperature transformations with our Ni- and Ti-rich films, respectively [21]. Subsequently, the NiTi films are coated with either a.) a bi-layer system of a sputter deposited Al_2O_3 buffer layer (10–20 nm) followed by a thermally evaporated Fe catalyst layer (1.1 nm, *buffered* samples) or b.) just with the Fe catalyst (*direct* samples). Samples are then subjected to thermal, atmospheric pressure CNT CVD, including pre-treatment in H_2/Ar (50:20, 3 min) and growth in C_2H_2/H_2/Ar (1:50:20, 30 min) at temperatures from 550 °C to 750 °C [23].

Scanning Electron Microscopy (SEM, FEI Philips XL30 sFEG, 2.5 kV, sample tilt ~60°) was employed to study sample morphology and composition via energy dispersive X-ray spectroscopy (EDX, 20 kV). CNTs were structurally characterised using Raman spectroscopy (Renishaw 1000 at an excitation wavelength of 633 nm). NiTi films were structurally investigated at room temperature before and after CVD by X-ray diffractometry (XRD) with a Bruker D8 (Theta–Theta scans, Cu-Kα radiation at 1.541 Å). Temperature dependent XRD was measured at the European Synchrotron Radiation Facility (beamline BM20/ROBL; Theta-2Theta, scans plotted at 1.541 Å; samples tilted by ~1° to suppress sapphire substrate reflections) with samples heated up to (100 ± 10)°C in ~10^{-1} mbar reduced pressure.

3. Results and discussion

We find that on all *buffered* samples CNTs were grown (Fig. 2(a)), where length, density and alignment of the tubes increase with increasing CVD temperature. This is consistent with common CNT growth temperature dependencies [23,24]. In contrast, *direct* samples show sparse CNTs at 550 °C but no CNT growth at higher temperatures. Only a roughened surface evolves, which is indicative of crystal growth in the NiTi [21]. This lack of growth on *direct* samples is ascribed to diffusion of the Fe catalyst into the NiTi, leading to depletion of the catalyst from the surface, hence preventing CNT growth. The Al_2O_3 buffer layer averts this catalyst diffusion [25,26] and is necessary to obtain μm-scale CNT forests on NiTi.

Fig. 2(b) shows the structural evolution of the *buffered* samples as measured by room temperature XRD. Before CVD, the non-annealed, room temperature sputter deposited NiTi shows a broad reflection ~43°, indicating only partial crystallisation [20]. Usually, NiTi films are either deposited onto heated substrates or post-deposition annealing is used to crystallize the NiTi into the desired martensitic/austenitic structure [2]. We find that our CNT CVD process fully substitutes for such annealing since the post-CVD 550 °C sample has been crystallised into austenite [27], as expected for annealed Ni-rich NiTi at room temperature [21]. With increased CVD temperature we observe

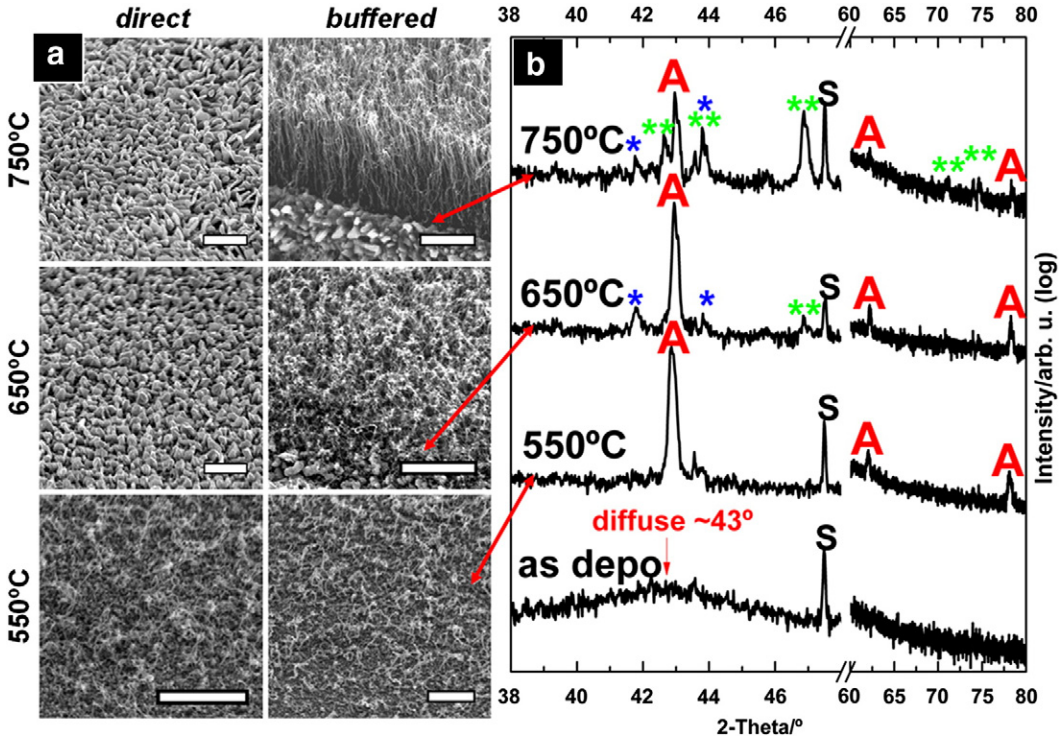

Fig. 2. (a) Typical CNT growth for *direct* and *buffered* (10 nm Al_2O_3) Ni-rich NiTi films at various CVD temperatures. (Scale bars: 1 μm) (b) Corresponding XRD scans of as deposited and post-CVD *buffered* samples. "A" designates austenitic NiTi reflections, "*" Ni_4Ti_3, "**" Ni_3Ti and "S" substrate related reflections [27].

further NiTi crystallization, however at the cost of formation of stoichiometric Ni_xTi_y precipitates ($x \neq 1$ and $y \neq 1$). We find Ni_3Ti and Ni_4Ti_3 formation at ~650 °C and a phase mixture (~1:1) between austenite and Ni_3Ti at 750 °C [27]. These precipitates are mainly undesirable in NiTi films for SME applications [3]. Hence, at higher CVD temperatures there is a trade-off between higher CNT yield and unwanted Ni_xTi_y precipitation. Further optimisation identified 625 °C as a good compromise. (Similar structural evolution is observed in *direct* samples, not shown).

The elevated temperatures and the highly reactive gases in CNT CVD can lead to unwanted structural changes in functional support materials, which can in turn render the support material useless [19]. In the case of NiTi as the CNT support, the formation of either Ni- or Ti-carbides (from C_2H_2) or oxides (from residual oxygen or adsorbed water in the CVD system) would inhibit SME properties. Therefore, it is important to note that none of our NiTi samples formed oxide or carbide phases during CVD. The films also did not develop cracks or delaminated, implying that mechanical stability of the NiTi films is not degraded by the CVD process.

To further prevent catalyst depletion into the NiTi we optimise the Al_2O_3 buffer layer thickness (as for Ti-rich NiTi in Fig. 3(a)) and find that doubling the buffer layer from 10 nm to 20 nm leads to a tenfold increase in forest height (to ~60 μm). This is because a thicker buffer layer increasingly suppresses the catalyst depletion from diffusion of Fe into the NiTi [25,26]. With these optimised CVD conditions (625 °C, 20 nm Al_2O_3) we obtain tens of μm high CNT forests on fully crystallised NiTi, as required in our proposed schematic. The CNTs are a mixture of multi- and single-walled CNTs (determined by Raman spectroscopy, not shown) at a surface density of ~10^9 CNTs/cm^2 (estimated from SEM).

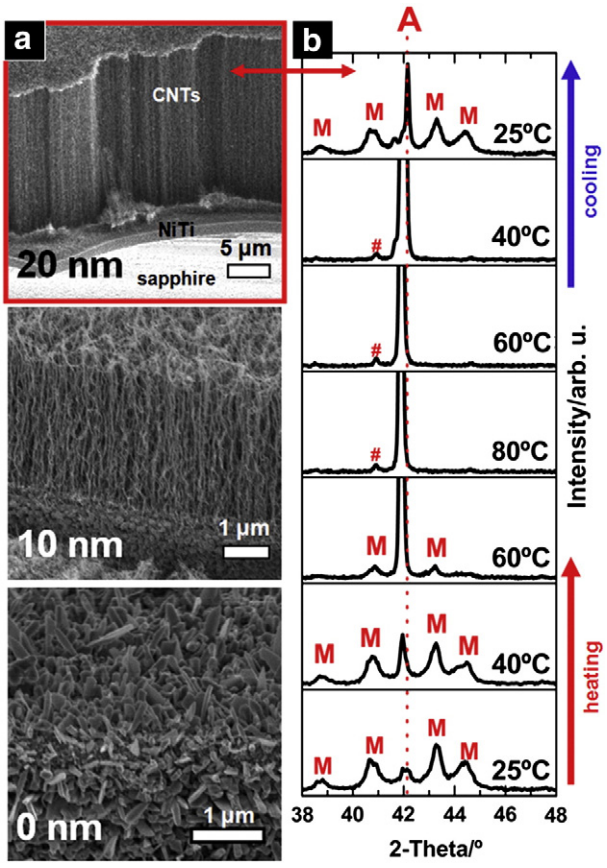

Fig. 3. (a) Typical CNT growth at 625 °C on Ti-rich NiTi with varying Al_2O_3 buffer thickness (0–20 nm). (b) Temperature dependent XRD scans of corresponding CNT covered 20 nm *buffered* Ti-rich sample, showing crystallographic response upon heating and cooling. "M" denotes martensitic and "A" austenitic NiTi reflections, respectively. "#" denotes a minor contribution from either remaining martensite or $NiTi_2$ [27]. Note that the intensity scale for all scans is fixed i.e. some austenite reflections are cut off.

We then evaluate whether, after CNT CVD, the SMA films still allow a reversible martensitic transformation, the basic crystallographic requirement to exploit SME properties. This is accomplished using temperature dependent XRD with CNT covered Ti-rich NiTi samples heated up to (100 ± 10)°C. Ti-rich NiTi is expected to be martensitic at room temperature and (reversibly) austenitic at ~>80 °C [21]. Indeed, at room temperature, our post-CVD sample is fully crystallised martensite with only a small austenite contribution (Fig. 3(b)). Upon heating to 40 °C, the austenite grows at the expense of the martensite, with an almost exclusively austenitic structure remaining at 80 °C. This is fully reversible to the initial martensite upon cooling (with a slight hysteresis). On this basis, we demonstrate that our forest CNT CVD conditions promote a microstructure in the NiTi that allows a reversible martensitic transformation, as required for SME exploitation.

While in this growth study we do not measure thermal properties or integrate the CNT–NiTi structures into MEMS devices to test the suggested enhanced thermal transport and cycling frequencies, we still may finally comment on the implications and current limitations of our growth results: In a first approximation, a μm-thick CNT layer is expected to dominate through-layer heat transport compared to nm-thick Al_2O_3 because of the direct proportionality between thermal resistance of a layer and its thickness [28]. Hence, the previously measured thermal conductivities of 3000–6000 W/Km [4,5] for single CNTs would imply ten times faster heat conduction between the SMA and a heat sink/source as compared to Cu, the benchmark thermal transport material for SMAs [3] (Cu ~400 W/Km, Al_2O_3 ~25 W/Km [29], NiTi ~15 W/Km [30]). This would imply a considerable increase in SMA cycling frequencies. However, previous studies have also reported a wide spread of thermal conductivity values for CNTs in forest form (0.4–1400 W/Km [9,10,13–16]). This is ascribed to insufficient CNT density, CNT defects and poor contacts to the CNTs in forest form [9]. These three parameters are still a subject of ongoing research and open to optimisation, which is by no means excluded by our proposed layer architecture and process flow. In fact, a very similar set of optimisation issues is found for the proposed use of CNTs in Ultra-Large-Scale-Integration (ULSI) vertical electrical interconnects [31]. As the μm-sized features in thermal management for MEMS circumvent many of the problems found in low-nm scale ULSI interconnects, many already established techniques, e.g. [32–35], will be directly applicable for further optimisation of CNTs on SMAs.

4. Conclusions

In summary, we propose to thermally contact SMA thin films with CNT forests to obtain faster actuation frequencies of the SMA films by enhanced heat transport through the CNTs. As a first step towards realisation of this concept, we achieve growth of CNT forests on the SMA material NiTi, without inhibiting its fully reversible martensitic transformation, fulfilling the basic requirement for SME exploitation. Future work is needed towards integration of these growth results into a CNT–SMA–MEMS test device to measure thermal transport properties and test the obtainable cycling frequencies.

References

[1] K. Otsuka, T. Kakeshita, MRS Bull. 27 (2002) 91.
[2] A. Ishida, V. Martynov, MRS Bull. 27 (2002) 111.
[3] Y. Fu, H. Du, W. Huang, S. Zhang, M. Hu, Sens. Actuators A 112 (2004) 395.
[4] P. Kim, L. Shi, A. Majumdar, P.L. McEuen, Phys. Rev. Lett. 87 (2001) 215502.
[5] S. Berber, Y. Kwon, D. Tomanek, Phys. Rev. Lett. 84 (2000) 4613.
[6] H. Lu, Y. Liu, J. Gou, J. Leng, S. Du, Appl. Phys. Lett. 96 (2010) 084102.
[7] X. Luo, P.T. Mather, Soft Matter 6 (2010) 2146.
[8] Z. Mo, J. Anderson, J. Liu, Proc. Sixth IEEE CPMT Conf. High Density Microsystems Design and Packaging and Component Failure Anlysis, HDP '04, 2004, p. 373.
[9] Y. Xu, Y. Zhang, E. Suhir, X. Wang, J. Appl. Phys. 100 (2006) 074302.

[10] H. Huang, C. Liu, Y. Wu, S. Fan, Adv. Mater. 17 (2005) 1652.
[11] K. Kordas, G. Toth, P. Moilanen, M. Kumpumaki, J. Vahakangas, A. Uusimaki, R. Vajtai, P.M. Ajayan, Appl. Phys. Lett. 90 (2007) 123105.
[12] Q. Ngo, B.A. Cruden, A.M. Cassell, G. Sims, M. Meyyappan, J. Li, C.Y. Yang, Nano Lett. 4 (2004) 2403.
[13] Y. Wu, C.H. Liu, H. Huang, S.S. Fan, Appl. Phys. Lett. 87 (2005) 213108.
[14] J. Xu, T.S. Fisher, Int. J. Heat Mass Transfer 49 (2006) 1658.
[15] X.J. Hu, A.A. Padilla, J. Xu, T.S. Fisher, K.E. Goodson, J. Heat Transfer 128 (2006) 1109.
[16] T. Iwai, H. Shioya, D. Kondo, S. Hirose, A. Kawabata, S. Sato, M. Nihei, T. Kikkawa, K. Joshin, Y. Awano, N. Yokoyama, IEEE International Electron Devices Meeting, IEDM Technical Digest, 2005, p. 257.
[17] I. Soga, D. Kondo, Y. Yamaguchi, T. Iwai, T. Kikkawa, K. Joshin, IEEE International Symposium on Radio-Frequency Integration Technology, 2009, p. 221.
[18] H.J. Dai, Acc. Chem. Res. 35 (2002) 1035.
[19] B.C. Bayer, S. Hofmann, C. Castellarin-Cudia, R. Blume, C. Baehtz, S. Esconjauregui, C.T. Wirth, R.A. Oliver, C. Ducati, A. Knop-Gericke, R. Schlögl, A. Goldoni, C. Cepek, J. Robertson, J. Phys. Chem. C. 115 (2011) 4359.
[20] S. Sanjabi, S.K. Sadrnezhaad, K.A. Yates, Z.H. Barber, Thin Solid Films 491 (2005) 190.
[21] S. Sanjabi, Z.H. Barber, Surf. Coat. Technol. 204 (2010) 1299.
[22] B.C. Bayer, A.F. Khan, M. Mehmood, Z.H. Barber, Thin Solid Films 518 (2010) 2659.
[23] C. Zhang, S. Pisana, C.T. Wirth, A. Parvez, C. Ducati, S. Hofmann, J. Robertson, Diamond Relat. Mater. 17 (2008) 1447.
[24] C.T. Wirth, C. Zhang, G. Zhong, S. Hofmann, J. Robertson, ACS Nano 3 (2009) 3560.
[25] A. Cao, P.M. Ajayan, G. Ramanath, R. Baskaran, K. Turner, Appl. Phys. Lett. 84 (2004) 109.
[26] J.M. Simmons, B.M. Nichols, M.S. Marcus, O.M. Castellini, R.J. Hamers, M.A. Eriksson, Small 2 (2006) 902.
[27] Powder Diffraction Files, JCPDS-International Centre for Diffraction Data; austenitic NiTi 65–5537, martensitic NiTi 35–1281, Ni_3Ti 51–1169, Ni_4Ti_3 65–3957, $NiTi_2$ 72–0442.
[28] H. Kuchling, Taschenbuch der Physik, 17th ed. Fachbuchverlag Leipzig im Carl Hanser Verlag, Munich, 2007.
[29] J.F. Shakelford, W. Alexander, CRC Materials Science and Engineering Handbook, 3rd ed. CRC Press, Boca Raton, 2001.
[30] W. Huang, Mater. Des. 23 (2002) 11.
[31] J. Robertson, G. Zhong, S. Hofmann, B.C. Bayer, C.S. Esconjauregui, H. Telg, C. Thomsen, Diamond Relat. Mater. 18 (2009) 957.
[32] D. Yokoyama, T. Iwasaki, T. Yoshida, H. Kawarada, S. Sato, T. Hyakushima, M. Nihei, Y. Awano, Appl. Phys. Lett. 91 (2007) 263101.
[33] J. Li, Q. Ye, A. Cassell, H.T. Ng, R. Stevens, J. Han, M. Meyyappan, Appl. Phys. Lett. 82 (2003) 2491.
[34] S. Esconjauregui, B.C. Bayer, M. Fouquet, C.T. Wirth, C. Ducati, S. Hofmann, J. Robertson, Appl. Phys. Lett. 95 (2009) 173115.
[35] S. Esconjauregui, M. Fouquet, B.C. Bayer, C. Ducati, R. Smajda, S. Hofmann, J. Robertson, ACS Nano 4 (2010) 7431.